

Unidentified Gamma-Ray Sources as Ancient Pulsar Wind Nebulae

O.C. de Jager*, S.E.S. Ferreira*, A. Djannati-Atai†, M. Dalton‡, C. Deil§, K. Kosack¶, M. Renaud†, U. Schwanke‡ and O. Tibolla§

*Unit for Space Physics, North-West University, Potchefstroom, South Africa

†Astroparticule et Cosmologie, Universite Paris 7 Denis Diderot, Paris, France

‡Institut fur Physik, Humboldt-Universitat zu Berlin, Berlin, Germany

§Max-Planck-Institut fur Kernphysik, Heidelberg, Germany

¶CEA Saclay, F-91191 Gif-sur-Yvette Cedex, France

Abstract. In this paper we explore the evolution of a PWN while the pulsar is spinning down. An MHD approach is used to simulate the evolution of a composite remnant. Particular attention is given to the adiabatic loss rate and evolution of the nebular field strength with time. By normalising a two component particle injection spectrum (which can reproduce the radio and X-ray components) at the pulsar wind termination shock to the time dependent spindown power, and keeping track with losses since pulsar/PWN/SNR birth, we show that the average field strength decreases with time as $t^{-1.3}$, so that the synchrotron flux decreases, whereas the IC gamma-ray flux increases, until most of the spindown power has been dumped into the PWN. Eventually adiabatic and IC losses will also terminate the TeV visibility and then eventually the GeV visibility.

I. INTRODUCTION

Aharonian et al. [1] discussed eight unidentified VHE gamma-ray sources discovered with the H.E.S.S. telescopes. All are extended objects with angular sizes ranging from approximately 3 to 18 arc minutes, lying close to the Galactic plane (suggesting they are located within the Galaxy). In each case, the spectrum of the sources in the TeV energy range can be characterized as a power-law with a differential spectral index in the range 2.1 to 2.5. The general characteristics of these sources (spectra, size, and position) are similar to previously identified galactic VHE sources (e.g. pulsar wind nebulae PWNe), however since these sources have so far no clear counterpart in lower-energy wavebands, further multi-wavelength study is required to understand the emission mechanisms powering them, and therefore follow-up observations with higher-sensitivity X-ray and GeV γ -ray telescopes will be beneficial (as stated in [1].)

One possibility is that we are dealing with relatively old PWN born from Type II supernovae, but still relatively close to the molecular clouds from which the massive progenitor stars were born. This will then also explain their proximity to the galactic plane.

A natural explanation would be that these sources were once bright in synchrotron emission, but that the field strength decreased with time as the PWN expanded

with time [2]: The pulsar eventually deposited all its spindown power into the nebula and whereas the synchrotron brightness decreased with time because of field decay, the inverse Compton γ -ray flux increases until reaching a convergent value, after which it will also decay because of continuous adiabatic losses and inverse Compton cooling. The γ -ray lifetime of a PWN can then be much longer than the apparent radio and X-ray lifetimes.

In this paper we will discuss the results of MHD and radiative modelling of evolving PWNe and show predicted evolutionary results for the composite SNR G21.5-0.9.

II. THE MHD MODEL FOR COMPOSITE SUPERNOVA REMNANTS

Supernova remnant evolution in either uniform or non-uniform media have been modelled extensively by e.g. [4], [5]. For either composite SNRs or PWNe in the ISM simulations were also presented by e.g. [6], [7], [8], [9], [10], [11]. In this work we use a similar model as used in most of the studies above by solving the well known Euler equations

$$\frac{\partial}{\partial t}\rho + \nabla \cdot (\rho\mathbf{v}) = 0, \quad (1)$$

$$\frac{\partial}{\partial t}(\rho\mathbf{v}) + \nabla \cdot (\rho\mathbf{v}\mathbf{v} + P\mathbf{I}) = 0, \quad (2)$$

$$\frac{\partial}{\partial t}\left(\frac{\rho}{2}\mathbf{v}^2 + \frac{P}{\gamma-1}\right) + \nabla \cdot \left(\frac{\rho}{2}\mathbf{v}^2\mathbf{v} + \frac{\gamma P\mathbf{v}}{\gamma-1}\right) = 0 \quad (3)$$

which describe inviscid flow. Here ρ is the density, \mathbf{v} the velocity and P the gas pressure. These equations describe the balance of mass, momentum and energy. Currently we only consider a one fluid scenario with an adiabatic index of 5/3. Although a relativistic description is necessary to model PWN evolution correctly, the speed of the relativistic material downstream of the pulsar wind termination shock is sufficiently smaller than c to use a non-relativistic treatment (see also e.g. [6]). The numerical scheme is discussed in [17] and compute solutions to hyperbolic differential equations using a wave propagation approach. See also [18] for more details. The model solves in spherical coordinates r and ϕ , with r ranging from 0.01 pc to 25 pc (2000 gridpoints) and ϕ from 0° to 180° (150 gridpoints).

For the initial and boundary conditions of the SNR (see also [12], [6], [8], [10]) we assume a spherical region, radius r_{ej} , and a high constant density ρ_{ej} with a radially increasing velocity profile

$$v = \frac{r}{t} = v_{ej}r/r_{ej}. \quad (4)$$

In this case we take $r_{ej} = 0.1$ pc while for the density we have

$$\rho_{ej} = \frac{3M_{ej}}{4\pi r_{ej}^3} \quad (5)$$

with M_{ej} the ejecta mass. For the velocity we have

$$v_{ej} = \sqrt{\frac{10}{3} \frac{E_{ej}}{M_{ej}}}. \quad (6)$$

To compute the PWN magnetic field we solve

$$\frac{\partial \mathbf{B}}{\partial t} + \nabla \times (\mathbf{v} \times \mathbf{B}) = 0 \quad (7)$$

using a similar scheme as for the fluid part. Note that this is not a full MHD solution because the field is calculated kinematically from the flow ([19], [20]) and no backreaction on the fluid is considered. More detailed MHD calculations were done by e.g [9] & [11].

III. CONSTRAINTS FROM PULSAR EVOLUTION

For the PWN we assume that the spin-down luminosity of the pulsar is given by (assuming a pulsar braking index of 3)

$$L(t) = \frac{L_0}{\left(1 + \frac{t}{\tau}\right)^2}, \quad (8)$$

where L_0 is the initial spindown power and τ the spindown timescale, which, for a birth period P_0 and present period P , is defined as

$$\tau = \frac{2\pi^2 I}{P_0^2 L_0} = \frac{2\pi^2 I P_0^2}{P^4 L}. \quad (9)$$

IV. THE EVOLUTION OF THE PLERIONIC MAGNETIC FIELD STRENGTH

To calculate the multiwavelength (MWL) spectrum we need to know the behaviour of the average PWN field strength $B(t)$ with time. This quantity was calculated by taking the volume averaged field strength between the pulsar wind termination shock radius and PWN outer radius.

The calculation of the average field strength starts progressively later (in time) with decreasing L_0 . This is because of the difficulty in resolving the position of the PWN termination shock as L_0 decreases. This difficulty should be resolvable if we reduce the grid size of the calculation, but at the expense of CPU calculation time. For example, the PWN termination shock radius of G21.5-0.9 is ~ 0.5 arcsec, corresponding to a shock radius of 0.01 pc, which is already consistent with the minimum assumed grid size.

Figure 1 shows the behaviour of the average $B(t)$ for L_0 ranging between 10^{38} to 10^{41} erg/s and ISM

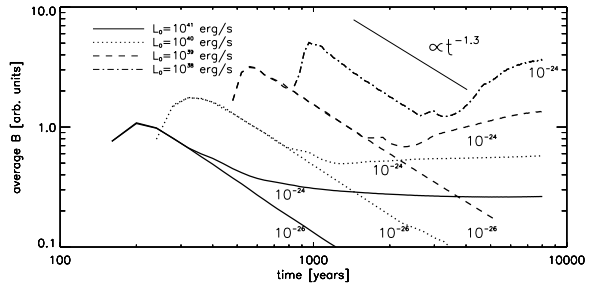


Fig. 1. The average magnetic field strength of the PWN for $\tau = 3000$ y and L_0 in the range as indicated. Two values of the ISM density was assumed. The slope $\propto t^{-1.3}$ indicates the approximate pre-reverse shock field decay evolution with time.

densities of 10^{-26} g/cm³ and 10^{-24} g/cm³. A more detailed discussion of this will be given elsewhere.

Prior to the passage of the reverse shock, we find that the field strength decreases as $t^{-1.3}$, independent of the chosen parameters. This is modified by the reverse shock, but after passage, the time evolution is expected to revert back to this $t^{-1.3}$ behaviour.

V. ADIABATIC LOSSES

In this section the evolution of a PWN inside a SNR is studied. Model solutions corresponding to $M_{ej} = 8M_{\odot}$ in Equation 5 and spin-down time $\tau = 3000$ y and $\tau = 300$ y in Equation 8 are shown. Different scenarios ranging from initial pulsar wind luminosity $L_0 = 10^{41}$ erg/s to $L_0 = 10^{38}$ erg/s in Equation 8 are shown.

The rate of change of the energy of a particle convected by a pulsar wind expanding at a velocity \vec{V} is given by

$$\frac{dE}{dt} = -\frac{E}{3}(\nabla \cdot \vec{V}) \quad (10)$$

Below we will see that this quantity is expected to be negative, giving rise to adiabatic losses, unless the PWN is sufficiently crushed by the reverse shock, such that the term $\nabla \cdot \vec{V} < 0$, in which case the particles will experience adiabatic heating. For practical purposes we calculate the average adiabatic energy loss rate over the PWN between the termination shock and PWN radii by averaging the quantity $\nabla \cdot \vec{V}$ over volume. The radius of the PWN was determined by establishing the position where the PWN field strength drops to zero. We scale the abovementioned rate of energy change (averaged over volume) by multiplying the relative energy loss rate $(dE/dt)/E$ with the age t of the PWN to give the dimensionless quantity $t(dE/dt)/E$. The results are shown in Figures 2a and 2b for spindown timescales of $\tau = 300$ y and $\tau = 3000$ y respectively and PSR/SNR parameters discussed above.

Initially we find that the quantity $t(dE/dt)/E$ is negative as a result of expansion, so that the particles lose energy due to this process. However, when the reverse shock compresses the PWN, we find that the quantity $\nabla \cdot \vec{V}$ becomes negative, in which case the particles will start to gain some of their lost energy.

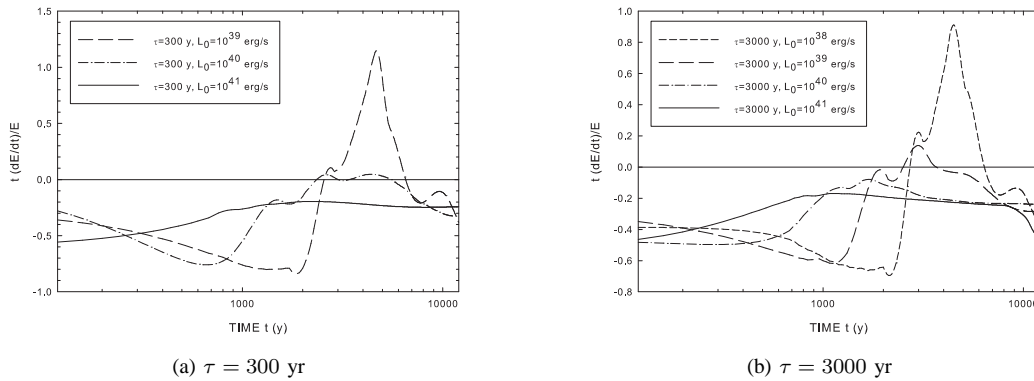


Fig. 2. The scaled relative energy loss rate $t(dE/dt)/E$ (a dimensionless quantity) due to adiabatic expansion as a function of time t since birth. The spindown timescale in this case is $\tau = 300$ y (left) and 3000 y (right), whereas the SNR ejecta mass for both cases was $8M_{\odot}$. The spindown power L_0 at birth is indicated in the Legend.

With decreasing L_0 we find that this heating process starts at progressively later times, since the time when the reverse shock encounters the PWN increases with such decreasing L_0 for the same τ .

It is interesting to note that the quantity $|t(dE/dt)/E|$ is always less than unity except when the reverse shock compresses the flow.

Since the relative adiabatic energy loss rate is nearly constant at a value around -0.5 (excluding the time of reverse shock passage), the total adiabatic losses of a particle injected during birth with initial energy E_0 and which can survive significant radiation losses would be

$$E \sim E_0 \left(\frac{t}{t_0} \right)^{-0.5}. \quad (11)$$

Note that $E = 0$ if $t_0 = 0$, which implies an inconsistent solution, unless $t_0 > 0$. We find that $t_0 \leq 100$ yr but we are currently reducing the grid size of the simulation and will report on the solution for a convergent value of t_0 in a followup paper.

VI. TIME DEPENDENT EVOLUTION OF THE LEPTON SPECTRUM

We define $N(E, t)$ as the time dependent differential particle spectrum for leptons of energy $E = \gamma m_e c^2$, whereas τ_{syn} and τ_{ad} are the timescales corresponding to synchrotron and adiabatic losses respectively. The magnetic field strength $B(t)$ (used in τ_{syn}) is time dependent. We then integrate the transport equation

$$\frac{dN}{dt} + \frac{N}{\tau_{\text{syn}}} + \frac{N}{\tau_{\text{ad}}} = Q(t) \quad (12)$$

between time $t = 0$ when $P = P_0$, i.e. the pulsar birth period and the current epoch at T_{SNR} assuming a pulsar braking index $n = 3$. From N we calculate the spectral energy distributions (SED) in synchrotron and inverse Compton as discussed below.

We adopt the injection spectrum of [16] for electrons at the pulsar wind shock

$$Q(E, t) = \begin{pmatrix} Q_0(t)(E/E_b)^{-p_1} & \text{for } E < E_b \\ Q_0(t)(E/E_b)^{-p_2} & \text{for } E_b < E < E_{\text{max}} \end{pmatrix}, \quad (13)$$

with E_b the intrinsic break energy between the radio and X-ray components. A value of $p_1 \sim 1.0$ reproduces the typical flat radio spectra, whereas $p_2 \sim 2$ would reproduce the uncooled spectral indices seen in X-rays at the pulsar wind termination shock.

Following [16], the energy equation for $Q(t)$ can be written in terms of the time dependent spindown power $L(t)$ giving

$$\int Q(\gamma, t) E dE = \eta L(t). \quad (14)$$

We will assume the conversion efficiency η of spindown power to particles as a free parameter. The total injected lepton energy over time t since birth is then (assuming a constant η)

$$W_e(t) = \int_0^t \eta L(t) dt = \eta \Delta E_{\text{rot}}, \quad (15)$$

where $\Delta E_{\text{rot}} = I(\Omega_0^2 - \Omega^2)/2$ (with $\Omega = 2\pi/P$) is the net kinetic rotational energy deposited between birth and time t .

VII. EVOLUTION TOWARDS AN UNIDENTIFIED GAMMA-RAY SOURCE

In our evolutionary model we will use the young composite SNR G21.5-0.9 as an example and follow the time evolution of the leptonic spectrum and hence MWL intensity. The central pulsar PSR J1833-1034 has a period of 61.8 ms and for an expansion age near 1 kyr [21], the spindown timescale τ should vary between 3000 and 3800 y given an inferred birth period P_0 between ~ 50 and 55 ms. The corresponding initial spindown power ranges between $L_0 = 5 \times 10^{37}$ and 10^{38} erg/s.

We will use $p_1 = 1$ as observed in radio [13] while for X-rays we would expect that a value of $p_2 = 2$

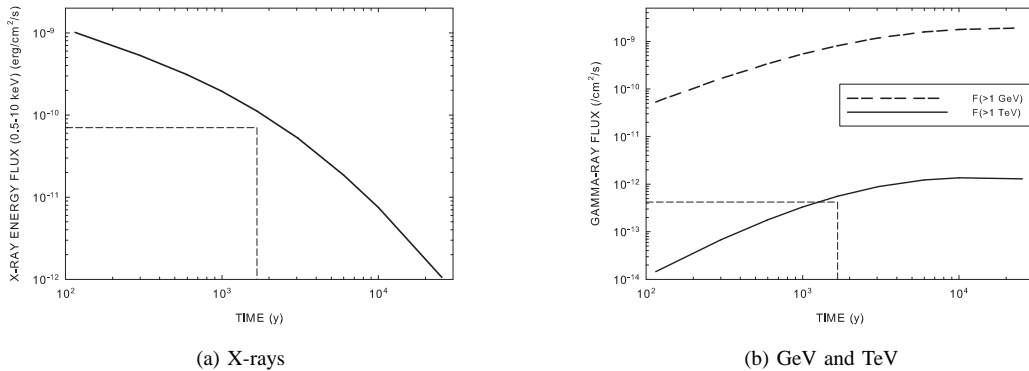


Fig. 3. The evolution of the X-ray (left) and GeV/TeV (right) fluxes with time. The dashed lines indicate the present state of G21.5-0.9.

corresponding to the pulsar wind termination shock [14] would reproduce the MWL spectrum best. However, an average value of $p_2 = 2.6$ seems to fit the data better.

To reproduce the ratio of energy fluxes between X-rays and TeV, we normalise the average field strength to $25\mu\text{G}$ at the present age near 1 kyr.

ISO observations [15] of the PWN show that the radio spectrum should break around 10^{12} Hz. This break is either intrinsic or due to radiation losses. We find however that this break cannot be due to radiation losses since this would imply a too large Crab-like field strength, which cannot be reconciled with the observed ratio of TeV to X-ray flux. An intrinsic break at energy E_b to $p_2 = 2.6$ best reproduces the post spectral break data.

For a birth period of $P_0 = 50$ ms we still need a relatively large conversion efficiency of $\eta = 0.7$ in eqn 14 to reproduce the observed synchrotron and IC spectra at the present epoch. The required break energy in eqn 13 is $E_b = 40$ GeV, which we will keep fixed with time since we have no theory on the evolution of E_b . The assumed radiation fields for the IC calculation were the CMBR, a 25K galactic dust component and starlight component corresponding to 1 eV/cm^3 . The latter two radiation energy densities agree approximately with the values found for the inner galaxy region at the location of G21.5-0.9 by [3].

Assuming a constant η with time, but the spindown power decreasing as that of a magnetic dipole, and hence decreasing particle input with time, we were able to calculate the time evolution of $Q(\gamma, t)$ and hence the MWL spectrum from which the time evolution of the radio, X-ray and TeV fluxes were calculated. The latter two are shown in Figure 3. It is clear that the X-ray flux decreases with time given the decreasing magnetic field strength with time, whereas both the inverse Compton GeV and TeV fluxes increases with time, reaching a limiting value. The predicted radio, X-ray and TeV fluxes agree with the observed fluxes at the present epoch.

VIII. CONCLUSIONS

In this paper we have given the basic ingredients which gives the time evolution of the MWL spectrum of a PWN. The basic result is the following: Whereas the X-ray flux is large during early epochs, the GeV and TeV fluxes start at relatively low values. As time progresses towards the Vela and post-Vela epoch, the synchrotron flux starts to decrease significantly, whereas the IC flux uncreases, until reaching a steady state value. Given the page limit of this paper, we could not explore the details of IC and adiabatic losses which would affect the time evolution at epochs $\gg 10$ kyr. This will be discussed in a followup paper.

The basic conclusion however remains, as a PWN grows older, it can remain bright in IC, whereas the GeV/TeV flux remains high. This can continue until IC and adiabatic losses, or, breakup and diffusion into the ISM finally terminates the gamma-ray lifetime.

REFERENCES

- [1] Aharonian, F. et al. 2008, A&A, 477, 353
- [2] de Jager, O.C., & Djannati-Ataï, A. 2008, 363rd Hereaus Meeting, arXiv:0803.0116
- [3] Porter, T.A., Moskalenko, I.V. & Strong, A.W. 2006, ApJL, 648, L29
- [4] Tenorio-Tagle, G. et al. 1991, MNRAS, 251, 318
- [5] Jun, B.-I. & Jones, T.W. 1999, ApJ, 511, 774
- [6] van der Swaluw, E. et al. 2001, A&A, 380, 309
- [7] Bucciantini, N. 2002, A&A, 387, 1066
- [8] Bucciantini, N. et al. 2003, A&A, 405, 617
- [9] van der Swaluw, E. 2003, A&A, 404, 939
- [10] Del Zanna, L., Amato, E., & Bucciantini, N. 2004, A&A, 421, 1063
- [11] Bucciantini, N., Amato, E., & Del Zanna, L. 2005, A&A, 434, 189
- [12] Blondin, J. M. & Ellison, D. C. 2001, ApJ, 560, 244
- [13] Salter, C.J. et al. 1989, ApJ, 338, 171
- [14] Slane, P. et al. 2000, ApJ, 533, L29
- [15] Gallant, Y.A. & Tuffs, R.J. 1998, Memorie della Societa Astronomica Italiana 69, 963
- [16] Venter, C. & de Jager, O.C. 2006, arXiv:astro-ph/0612652.
- [17] LeVeque, R. J. 2002, Finite Volume Methods for Hyperbolic Problems (Cambridge University Press)
- [18] Ferreira, S.E.S. & de Jager, O.C. 2008, A&A, 478, 17
- [19] Scherer, K. & Ferreira, S.E.S. 2005, Astrophysics and Space Sciences Transactions, 1, 17
- [20] Ferreira, S.E.S. & Scherer, K. 2006, ApJ, 642, 1256
- [21] Bietenholz, M.F. & Bartel, N. 2008, MNRAS, 386, 1411